Author(s): Alava, Mikko J. & Dubé, Martin

Title: Droplet spreading and pinning on heterogeneous substrates

Year: 2012

Version: Final published version

Please cite the original version:

Alava, Mikko J. & Dubé, Martin. 2012. Droplet spreading and pinning on heterogeneous substrates. Physical Review E. Volume 86, Issue 1. 011607/1-6. ISSN 1539-3755 (printed). DOI: 10.1103/physreve.86.011607.

Droplet spreading and pinning on heterogeneous substrates

Mikko J. Alava
Aalto University, Department of Applied Physics, PO. Box 14100, 00076 Aalto, Finland

Martin Dubé
Centre de Recherche sur les Matériaux Lignocellulosiques, Université du Québec à Trois-Rivières, Trois-Rivières, Canada G9A 5H7

(Received 12 July 2010; revised manuscript received 9 July 2011; published 30 July 2012)

The contact angle of a fluid droplet on an heterogeneous surface is analyzed using the statistical dynamics of the spreading contact line. The statistical properties of the final droplet radius and contact angle are obtained through applications of depinning transitions of contact lines with nonlocal elasticity and features of pinning-depinning dynamics. Such properties not only depend on disorder strength and surface details, but also on the droplet volume and disorder correlation length. Deviations from Wenzel or Cassie-Baxter behavior are particularly apparent in the case of small droplet volumes and small contact angles.

DOI: 10.1103/PhysRevE.86.011607 PACS number(s): 68.08.Bc, 47.55.dr, 64.60.Ht

I. INTRODUCTION

Liquid droplets on solid surfaces pose several interesting theoretical and experimental challenges and have a direct importance in several industrial processes. In general, the interaction of the liquid with the surface is characterized through the contact angle that a droplet, with known volume, makes with the surface. For a flat, chemically homogeneous surface, the equilibrium contact angle is easily obtained from an energy minimization procedure. The result, known as Young's law, includes the three surface energies (solid-liquid, solid-vapor, liquid-vapor, γ_{sl}, γ_{sv}, γ, respectively) with a "weight factor" for the last one, the cosine of the contact angle, $\cos\theta$. The dynamical approach to equilibrium is also well understood, both for complete [1] and partial [2] wetting. In reality, the static contact angle, as well as its dynamics, is obviously influenced by the variations in the physicochemical or geometrical properties of the substrate on which the droplet spreads [1,3–5]. Such surfaces are present in an enormous variety of industrial processes. Typical examples range from printing and coating to painting, as well as the creation of tailored superhydrophobic surfaces [6].

The static contact angles for surfaces with local variation can be obtained from variants of the original energy minimization. The classic Cassie-Baxter treatment for spatially varying surface energies considers a simple spatial average, i.e., $\langle\gamma(r)\rangle$ [7]. Likewise, Wenzel law for surfaces with height variations introduces the ratio—always larger than unity—of the total surface to the projected surface as a correction factor [8]. Clearly both Cassie-Baxter and Wenzel treatments may not apply in practice, since a droplet spreading towards equilibrium will encounter several pinning states in which it can be trapped, thereby never reaching the theoretical result [9,10]. This is a much-studied issue both experimentally and theoretically, particularly for engineered surfaces [11–14]. Approaches that have been tried range from hydrodynamic simulations of spreading to quasistatic considerations [15,16]. In all cases, a crucial concept is the spreading power, or the difference of the actual contact angle from the static or equilibrium one.

Here we analyze the consequences of surface heterogeneity on the spreading and final static state of liquid droplets. Our approach centers on the evolution of the droplet radius, as defined by the contact line that separates the wetted and nonwetted parts of the substrate. The radii are then easily related to values of contact angle through volume conservation. The droplet radius evolves under the influence of three factors: (i) the imbalance in surface tension, directly related to the spreading power, (ii) the quenched noise, induced by the locally varying surface properties, that introduces angular deformation in the radius, and (iii) contact line elasticity that tends to smoothen radius angular variations.

We use contact line pinning and depinning dynamics to follow the evolution of the droplet radius. In the initial stages of spreading, surface tension imbalance controls the dynamics. However, as the droplet spreads, disorder effects start to dominate and the contact line comes to a halt *before* an equilibrium state can be reached. Disorder, elasticity, and spreading thus predict a *pinning transition* for the contact line, and thus a droplet *pinning radius* that is sample-dependent. We show how this depends on the the independent parameters of the theory: disorder strength, disorder length-scale, droplet radius and volume, and the fluid properties such as surface energy and contact angle.

We further obtain the statistical distributions of the pinning radius. Small droplets are strongly effected by disorder, leading to results that are markedly different from what could be expected within a Wenzel or Cassie-Baxter framework. Disorder effects are apparent in the case of droplets with a small contact angle and disorder variations that are correlated on a short length scale with respect to the droplet radius. The pinning predictions for the contact angle have simple experimental consequences: they can be tested by varying for a given type of surface the nominal contact angle (by changing liquid for instance) and by varying the droplet size.

The rest of this paper is structured as follows. In Sec. II we outline the basic spreading phenomena as well as the approach to the pinning phase. Droplet spreading in the pinning phase is analyzed in detail in Sec. III, and Sec. IV finishes with conclusions.

II. DROPLET SPREADING AND APPROACH TO PINNING

We consider a liquid droplet with air-liquid interfacial tension γ, density ρ, and viscosity η deposited on a

macroscopically flat surface. When the size of the droplet is smaller than the capillary length $(\gamma/\rho g)^{1/2} \sim 1$ mm, the droplet has the overall shape of a spherical cap with basal radius R, the air-liquid interface joining the solid surface with contact angle θ. For a perfectly homogeneous surface, the equilibrium contact angle $\theta_{\rm eq}$ can be obtained from Young's law:

$$\gamma \cos\theta_{\rm eq} = \gamma_{sv} - \gamma_{sl}, \tag{1}$$

related to the equilibrium radius $R_{\rm eq}$ via the drop volume Ω:

$$\Omega = \frac{\pi}{3}\frac{R^3}{\sin^3\theta}(2 - 3\cos\theta + \cos^3\theta). \tag{2}$$

This relation reduces to $\Omega = \pi R^3\theta/4$ for small contact angles $\theta \ll 1$.

Equation (1) has to be supplemented by a correction term involving the line tension τ, related to κ, the curvature of the contact line [17,18]

$$\cos\theta = \cos\theta_{\rm eq} + \frac{\tau}{\gamma}\kappa. \tag{3}$$

The actual value of the line tension remains a difficult quantity to measure, due to chemical or topographical heterogeneity of the substrate and the difficulty to perform experimental work with sub-micron-sized droplets. In general, the value of the line tension can be estimated to be $\tau \sim 10^{-10}N$, thus representing a relevant correction only for droplets with nanometer range dimensions.

Substrate disorder induces variations in the contact line and hence in the local values of the contact angle and radius of the droplet. If x is the local coordinate along the contact line, the local droplet radius is $R(t) + h(x,t)$, where $R(t)$ is the spatially averaged radius. Variations along the contact line are connected to variations of the local contact angle $\theta(x,t)$, since the overall volume of the drop is conserved. To first order in the radius variations, the variations in the contact angle are [1,19]

$$\theta(x,t) = \theta(t)\left(1 + \int dx' \frac{h(x',t)}{(x-x')^2}\right). \tag{4}$$

Correction terms coming from the overall curvature of the droplet can be neglected for small variations of the contact line.

Upon deposition on a surface, a droplet will tend to its equilibrium shape through hydrodynamical spreading, under the influence of uncompensated Young's force $\mathcal{S}_y(\theta(x,t))$ and disorder variations $\mathcal{S}_d(\theta(x,t))$ [1],

$$\frac{3\eta l}{\gamma}\left(\frac{dR(t)}{dt} + \frac{dh(x,t)}{dt}\right) = \mathcal{S}_y(\theta(x,t)) + \mathcal{S}_d(\theta(x,t)), \tag{5}$$

where l is a numerical factor arising from finite slip at the contact line [1].

For small values of the contact angle $\theta \ll 1$ and to first order in contact line deviations [using Eq. (4)], the uncompensated Young force, corrected with a term arising from the dissipation at the contact line [1],

$$\mathcal{S}_y(\theta(x,t)) = \tan(\theta(x,t))[\cos(\theta_{\rm eq}) - \cos(\theta(x,t))], \tag{6}$$

is decomposed into an overall term independent of contact line variations and a nonlocal term,

$$\mathcal{S}_y(\theta(x,t)) = S(\theta(t)) + S_{\rm el}(\theta(t),h(x,t)), \tag{7}$$

where the spreading power,

$$S(\theta) = \theta\left(\theta^2 - \theta_{\rm eq}^2\right), \tag{8}$$

is balanced by the elastic restoring force,

$$S_{\rm el}(\theta,h(x,t)) = \theta\left(3\theta^2 - \theta_{\rm eq}^2\right)\int dx' \frac{h(x',t)}{(x-x')^2}. \tag{9}$$

For simplicity, we consider a chemically disordered substrate, which contributes a quenched random force. Again, in the limit $\theta \ll 1$ and to first order in the contact line variations,

$$S_d(\theta) = \frac{\theta}{\gamma}\delta\gamma(h(x,t)), \tag{10}$$

where

$$\delta\gamma(x,h(x)) = \delta\gamma_{sv}(x,h(x)) - \delta\gamma_{sl}(x,h(x)). \tag{11}$$

The noise is generally delta-correlated over two microscopic scales $\xi_\parallel$, $\xi_\perp$, parallel and perpendicular to the direction of spreading, dependent on the nature of the substrate. It includes the chemical contrast (via the variation of the surface energies, γ_{sv} and γ_{sl}, where the indices denote the solid-vapor and solid-liquid cases, respectively) and may also include surface roughness through local surface tilts [1,20]. In what follows, we consider the slowly evolving dynamics of the drop. This can be achieved experimentally by slowly depositing a droplet on the substrate, thereby avoiding initial impaction effects. After that, the viscous contact line dynamics dictates the (slow) evolution of the droplet [21]. The analysis does not apply to volatile liquids and the Ohnesorge number $Oh = \eta/(\rho R\gamma)$ is an appropriate parameter to estimate how viscous the liquid must be in order to prevent inertial as well as front instability (coming from evaporation) effects to occur [22]. We only consider microscopic disorder such that the length scales $\xi_\parallel$ and $\xi_\perp$ are the smallest length scales of the problem. The droplet then globally keeps a spherical shape, with disorder inducing variations in the contact line itself.

On a disordered surface, the equilibrium contact angle of a droplet may be markedly different from the prediction of Eq. (1), depending on the type or disorder. For example, bimodal chemical disorder, where a fraction f of the surface has surface tension $\gamma + \Delta\gamma$, is usually analyzed in terms of Cassie-Baxter equation,

$$\cos\theta_{\rm [CB]} = \cos\theta_{\rm eq} - f\frac{\Delta\gamma}{\gamma}, \tag{12}$$

which is essentially a weighted average of the equilibrium contact angle on each surface. On the other hand, topographical disorder (surface roughness) is encompassed within Wenzel's result,

$$\cos\theta_W = A_r\cos\theta_{\rm eq}, \tag{13}$$

where the relative area $A_r > 1$ is the ratio of the total surface to the projected surface under the drop (see [23,24] for recent similar analyses). It is interesting to note that, through Wenzel's analysis, roughness increases the wetting or nonwetting tendencies originally present in the problem, i.e., if $\theta_{\rm eq} < \pi/2$, $\theta_W < \theta_{\rm eq}$ until $\cos\theta_{\rm eq} = 1/A_r$ at which point a wetting film should be formed.

Both approaches however neglect that spreading is a dynamical phenomenon and that a droplet may become pinned

in several configurations before reaching equilibrium. Spatial scales and correlations of the disorder are also not included.

During spreading, the contact line roughens due to the quenched disorder of the substrate, a phenomenon analyzed extensively in the literature [20,25–27], also in the context of the hysteresis for advancing and receding contact lines [28]. When disorder becomes relevant the interface dynamics enters a critical regime where pinning occurs, and the interface propagates through avalanches. This regime is characterized by a force F_c, at which an interface becomes pinned. Around F_c, the contact line develops local self-affine fluctuations (roughness) $w \sim r^{\zeta}$ where r is the length of the interface and $\zeta \sim 0.38$ the roughness exponent specific to contact line motion [29–31].

The propagation of the interface by avalanche is characterized by a series a correlation lengths and critical exponents. During the avalanche, a portion of the avalanche, with lateral size ξ, moves by a distance $w \sim \xi^{\zeta}$. The duration $\tau \sim \xi^{z}$ of the interface is characterized by the dynamical exponent z. The lateral extent of the avalanches is a correlation length related to the driving force F and the pinning force F_c by the critical exponent ν: $\xi \sim (F - F_c)^{-\nu}$. Finally, the velocity of the interface scales as $v \sim (F - F_c)^{\beta}$. Critical scaling implies that $\beta = \nu(z - \zeta)$ and, for nonlocal elastic interface, $\nu = (1 - \zeta)^{-1}$. Again, for the specific case of contact line motion $\beta \sim 0.625$ [32].

For any finite system, F_c and thus the corresponding critical angle θ_c have a finite-size correction and in particular a sample (and disorder) -dependent actual critical value, with an universal probability distribution. This distribution is characterized by its width which decays with the interfacial length and depends only on the strength of the disorder, measured by the prefactor of the disorder two-point correlation function [33].

Although a complete solution of roughening requires additional nonlinear terms, Eq. (5), together with typical scaling arguments [20,26], already provides much information. Balancing the elastic restoring force [Eq. (9)] against disorder [Eq. (10)] yields a length scale $l_c = \xi_{\perp}(3\theta^2 - \theta_{\rm eq}^2)^2\gamma/\Gamma$, where $\Gamma = (\delta\gamma)^2/\gamma$ describes the pinning strength of disorder. For length scales $l \ll l_c$, the elastic restoring force dominates while disorder dominates for $l \gg l_c$. The contact angle θ_p at which pinning first becomes relevant is then obtained by balancing the spreading power [Eq. (8)] against either the elastic or pinning force at the length scale l_c. To first order in $(\theta_p - \theta_{\rm eq})/\theta_{\rm eq}$,

$$\theta_p = \theta_{\rm eq} + \frac{1}{\theta_{\rm eq}^3}\frac{\Gamma}{\gamma}. \tag{14}$$

Through volume conservation (using $\Omega = \pi R^3\theta/4$), this translates to a pinning radius

$$\frac{1}{R_p^3} = \frac{1}{R_{\rm eq}^3} + \frac{1}{\theta_{\rm eq}^3}\frac{\Gamma}{\gamma}\frac{\pi}{4\Omega}. \tag{15}$$

The volume of the droplet thus plays a crucial role. Large droplets will enter the pinning regime already close to equilibrium while, for smaller droplets, the ratio $R_p/R_{\rm eq}$ can be much smaller than 1, even more so for strong wetting $\theta_{\rm eq} \ll 1$.

III. SPREADING IN THE PINNED PHASE

We now consider spreading on a disordered substrate. The case of a contracting droplet (for equilibrium contact angles in excess of $\pi/2$) is an easy extension not reported here. The droplet has initial basal radius $R_0 \ll R_{\rm eq}$ and increases its radius through hydrodynamical spreading until R_p. Then, disorder becomes relevant and spreading continues if the spreading power [cf. Eq. (8)] at position R, $S(R > R_P)$, can overcome the combined pinning potential coming from the disordered substrate and the elastic restoring force, denoted S_c. At the first pinning radius, the spreading power

$$S_p \equiv S(R_p) = \left(\frac{4\Omega}{\pi}\right)^3 \frac{1}{R_p^3}\left(\frac{1}{R_p^6} - \frac{1}{R_{\rm eq}^6}\right) \sim S_0(R_{\rm eq} - R_p), \tag{16}$$

where the last form is in the limit $(R_{\rm eq} - R_p)/R_{\rm eq} \ll 1$ with $S_0 = 6\theta_{\rm eq}^3/R_{\rm eq}$. S_p corresponds to a contact angle value θ_p. In the similar limit, the elastic and disorder-induced forces can be written

$$S_{\rm el} + S_d = 2\theta_{\rm eq}^3 \int dx' \frac{h(x',t)}{(x - x')^2} + \frac{\theta_{\rm eq}}{\gamma}\delta\gamma(h(x,t)). \tag{17}$$

An analysis of spreading to a radius past R_p necessitates the knowledge of the pinning force distribution resulting from Eq. (7). Extensive numerical simulations of a driven interface subjected to the combined elastic-disorder force [Eq. (17)] have shown that the probability $F(S(r))$ of propagating past a radius r derives from a distribution of pinning forces for an interface of length r, $f(s_c,r)$ [34,35],

$$F(S(r)) = \int_0^S ds_c f(s_c,r) = 1 - \int_S^{S_p} f(s_c,r)ds_c. \tag{18}$$

The distribution follows a scaling form

$$f(s_c,r) \sim \left(\frac{r}{\xi_{\parallel}}\right)^{1-\zeta} \psi\left[\left(\frac{S_p - s_c}{S_p}\right)\left(\frac{r}{\xi_{\parallel}}\right)^{1-\zeta}\right], \tag{19}$$

with a scaling function $\psi(f)$ independent of the details of the disorder [35]. Close to pinning, $(S_p - s_c)/S_p \ll 1$, the scaling function has a power law behavior, $\psi(f) \sim f^{\gamma}$ with $\gamma = \zeta/(1 - \zeta)$.

In this critical regime, the likelihood $P(R)$ that the droplet radius will at least be R is obtained from a probabilistic argument, an approach also used for indentation crack propagation [34]. The motion of the droplet (see Fig. 1) consists of a succession of steps over independent configurations of the pinning disorder—i.e., the distance covered is divided into uncorrelated increments. The size of the steps can be inferred from the critical dynamics of the contact line motion. After step i, during the sequence of jumps, the pinned contact line explores the combined potential (elastic plus disorder) over a distance $w(R)$, finding a configuration that tend to minimize its energy. Upon depinning (i.e., step $i + 1$), the contact line moves, by a distance $w(R)$ [25,26], into a new configuration. At this point, both the contact line configuration as well as the combined potential are completely uncorrelated with the previous one. The appropriate step size during the sequence of events is thus $w(R)$, the roughness of the contact line. A

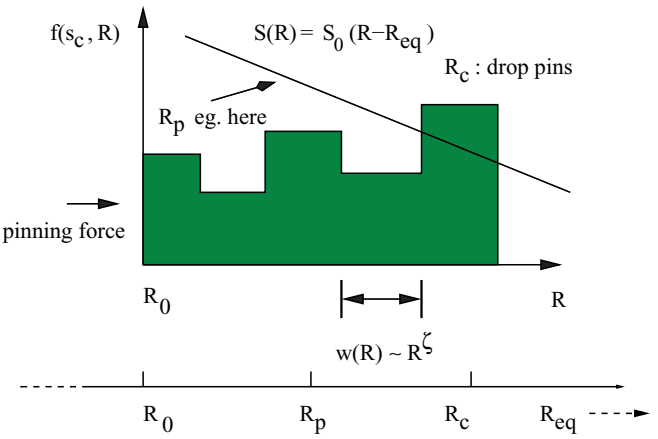

FIG. 1. (Color online) Schematic of the motion through jumps over independent pinning shells of a size (roughness) $w \sim R^{\zeta}$. At each shell, the local critical force follows the distribution of Eq. (19). The global driving force decreases as the spreading proceeds.

droplet will thus reach a given $R(t)$ if it has passed through all the previous pinning zones without being stopped. The probability of such a chain of events is

$$P(R) = \prod_i F(S(R_p + i/\lambda) > S_c), \tag{20}$$

where $F(S(r) > S_c)$ is the probability that the spreading power at radius r is larger than the pinning spreading power S_c. Time is not explicitly included in this argument. In the continuous limit, Eq. (20) can be rewritten

$$P(R) \approx \exp\left[\int_{R_p}^{R} \ln\left[F(S(r))\right] \lambda(r) dr\right], \tag{21}$$

where the zone size $1/\lambda$ is related to the droplet radius and the correlation lengths of the disorder, $\frac{1}{\lambda(R)} \propto \xi_{\perp}(\frac{R}{\xi_{\parallel}})^{\zeta}$.

For a droplet size large as compared to the scale of heterogeneities, effective contact angle values will always remain in the immediate vicinity of θ_p and the power-law behavior of ψ at the origin can be used to approximate $\ln[F(S(r))] \propto -\frac{r}{\xi_{\parallel}}(\frac{S_p - S}{S_p})^{\frac{1}{1-\zeta}}$, which leads to

$$P(R) \approx \exp\left\{-A R_p^{2-\zeta} \int_{R_p}^{R} \left(\frac{r}{R_p}\right)^{1-\zeta} \left(\frac{S_p - S(r)}{S_p}\right)^{\frac{1}{1-\zeta}} \frac{dr}{R_p}\right\}, \tag{22}$$

where the prefactor $A \propto \frac{\xi_{\parallel}^{\zeta-1}}{\xi_{\perp}}$ depends only on the material parameters through the correlation lengths of the disorder $\xi_{\parallel}$ and $\xi_{\perp}$. The use of the linearized form for the spreading power, Eq. (16), and a change of variable $x = R/R_p$ finally yields

$$P(x R_p) \approx \exp\left\{-A B^{-\frac{1}{1-\zeta}} R_p^{2-\zeta} \int_1^x du\, u^{1-\zeta} (u-1)^{1/(1-\zeta)}\right\}, \tag{23}$$

with $B = R_{\rm eq}/R_p - 1$. The integral in Eq. (23) exhibits a universal form which only depends on A, a disorder scale parameter, and R_p, related to $R_{\rm eq}$ and the strength of the disorder through Eq. (15). The size of the droplet is thus implicitly present in Eq. (23).

To analyze the results, it is convenient to set $\xi_{\perp} = \xi_{\parallel} \equiv \xi$. The relevant dimensionless ratios are then $R_p/R_{\rm eq}$, a measure of the influence of disorder strength, droplet volume, and equilibrium wetting properties, and $R_{\rm eq}/\xi$, which relates the droplet typical size to the spatial structure of the disorder. These ratios are made apparent from the limit $x \gg 1$ of Eq. (23) which reads

$$\ln[P(R \gg R_p)] \sim -\left(\frac{R_{\rm eq}}{\xi}\right)^{2-\zeta} \left(\frac{R_{\rm eq}/R_p}{(R_{\rm eq}/R_p) - 1}\right)^{\frac{1}{1-\zeta}} \times \left(\frac{R}{R_{\rm eq}}\right)^{2-\zeta+\frac{1}{1-\zeta}}. \tag{24}$$

The probability for the droplet to reach a given R thus decays quickly close to R_p. This decay is sharper for drops that are large compared to the disorder scale ($R_p \gg \xi$) than for smaller drops. This tendency to cluster around R_p drastically increases as the ratio $R_{\rm eq}/R_p \to 1$, which occurs for weak disorder or very large drops.

The importance of the ratio R_p/ξ is clearly shown in Fig. 2, where the probability to reach a radius R as calculated from Eq. (23) is shown for various ratios R_p/ξ and $R_p/R_{\rm eq}$. For values $R_p/\xi \gg 1$, this probability drops sharply and the drop remains essentially pinned at a radius R_p. It is only for relatively small values of this ratio that the probability to reach a radius larger than R_p increases significantly. In other words, occasionally for small droplets the spreading can get closer to the equilibrium radius.

The effect of disorder on the values of contact angles at pinning can then be elaborated by comparing the predicted value to $\theta_{\rm eq}$ using volume conservation, Eq. (2). Figure 3 shows the average contact angles calculated from the theory for two values of $\theta_{\rm eq}$. At large values of the ratio $R_{\rm eq}/\xi$, the final value of the contact angle is essentially determined by the value of R_p, i.e., strong disorder, characterized by a small ratio $R_p/R_{\rm eq}$ leads to a larger apparent contact angle. In such a case, it is

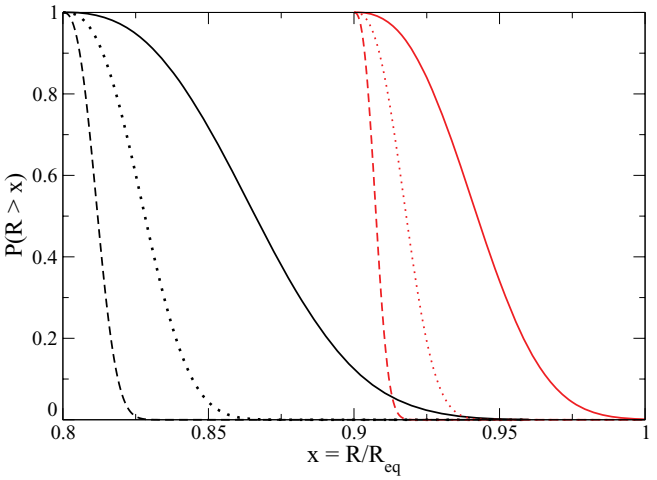

FIG. 2. (Color online) Probability for the droplet to reach a given radius R. The probability $P(R) = 1$ until $R = R_p$ after which it decays depending on the values of the ratios R_P/R_{eq} and R_{eq}/ξ. Solid, dotted, and dashed lines respectively correspond to $R_{\rm eq}/\xi = 25$, 100, and 400, while two values, $R_p/R_{\rm eq} = 0.8$ (left set of curves) and $R_p/R_{\rm eq} = 0.9$ (on the right) are used.

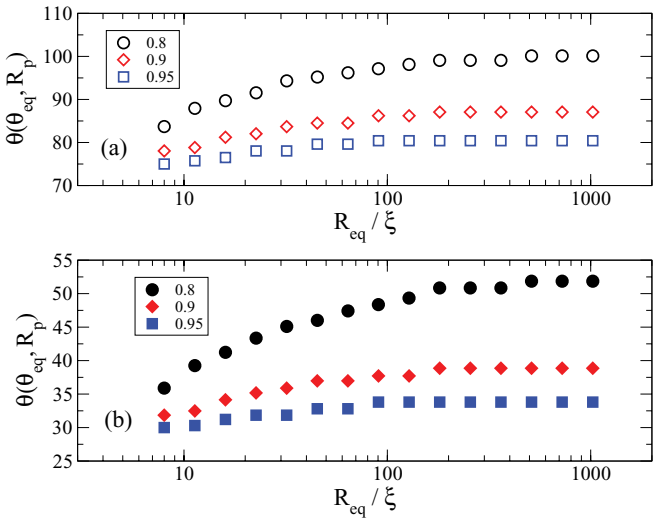

FIG. 3. (Color online) Average values of the contact angle at pinning for (a) $\theta_{\rm eq} = 75^\circ$ and (b) $\theta_{\rm eq} = 30^\circ$. The contact angle is shown as a function of $R_{\rm eq}/\xi$ for three ratios $R_p/R_{\rm eq} = 0.8, 0.9$, and 0.95.

only for a small value of the ratio $R_{\rm eq}/\xi$ that the apparent contact angle can be quantitatively close to the expected $\theta_{\rm eq}$.

In Fig. 4 we show for three different disorder (Γ) values how $R_p/R_{\rm eq}$ itself scales for various contact angles and a fixed ξ taken to be 10 micrometers. The values of Γ are taken to have representative values; note that the parameter measures the relative variation of the surface energy due to chemical disorder or due to roughness. Out of a variety of cases, we depict nine representative ones to show the trends. Figure 4(a) shows the actual droplet volumes at hand for each contact angle and disorder, while Fig. 4(b) shows the ratios of the pinning radius to the equilibrium one. The trends themselves are obvious (larger contact angles lessen the effect of pinning, while stronger disorder works to the other direction), and the

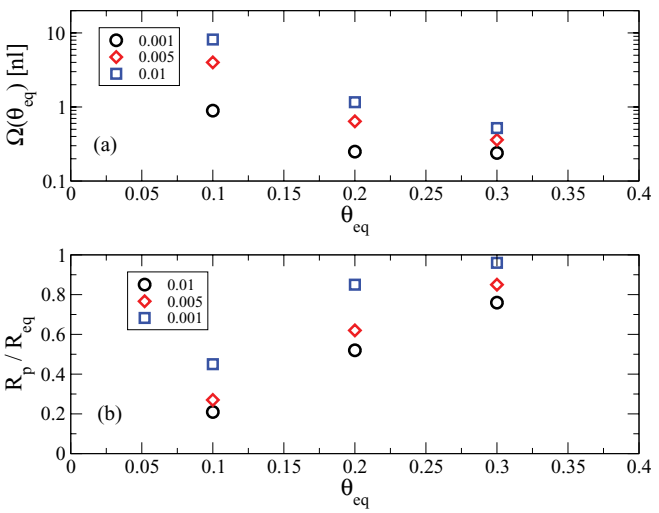

FIG. 4. (Color online) Volumes of droplets in nanoliters as a function of contact angle (in degrees, the values are from 5.7° to 18.1°) and disorder strength Γ (a). (b) The resulting values of $R_p/R_{\rm eq}$. The disorder scale ξ is set to 10 μm.

final prediction is then to be computed similarly to Fig. 3 for all the cases, separately.

It is thus interesting to note that the wetting properties of the surface, present through $\theta_{\rm eq}$, also enter explicitly the problem through the values of R_p and $R_{\rm eq}$. This is in contrast with Wenzel law or Cassie law which relate the apparent contact angles to the equilibrium contact angle through a set of constants independent of the nature of the surface or of the liquid. For naturally wetting surfaces ($\cos\theta_{\rm eq} > 0$), Wenzel law predicts that the apparent contact angle is *larger* than the equilibrium contact angle. This however neglects the fact that spreading is a dynamical process and that pinning of the contact line impedes the droplet from reaching an equilibrium state.

The temporal aspects of the radial pinning process can be obtained from the relation between the interface velocity and the driving force in the critical regime. Hydrodynamical spreading of the droplet occurs until the droplet reaches the radius R_p, at time $T_p \sim (R_p/R_{\rm eq})^9 (R_p\eta/\gamma)/\theta_{\rm eq}^3$. At this point, the spreading velocity $V_p \equiv V(R_p) = \gamma\theta_p(\theta_p^2 - \theta_{\rm eq})/r\eta l$.

After this point, motion proceeds by avalanches, with a velocity

$$V(R) = V(R_p)\left(\frac{R_{\rm eq} - R}{R_{\rm eq} - R}\right)^{\beta}, \tag{25}$$

where again $\beta \sim 0.62$. The time needed to move across a given shell of thickness $\lambda^{-1}(r)$ is simply $\Delta T(r) = \lambda^{-1}(r)/V(r)$ and the total time to pinning is obtained from summing the successive contributions of each shells. In the continuous limit, $T(R) = T_p + \frac{(R_{\rm eq}-R)^\beta}{V_p}\int_{R_p}^{R}\frac{1}{(R_{\rm eq}-r)^\beta}dr$, which is calculated to

$$T(R) = T_p + \frac{1}{1-\beta}\frac{R_{\rm eq}}{V_p}\left(1 - \frac{R_p}{R_{\rm eq}}\right)^{\beta}\left[\left(1 - \frac{R_p}{R_{\rm eq}}\right)^{1-\beta} - \left(1 - \frac{R}{R_{\rm eq}}\right)^{1-\beta}\right] \tag{26}$$

and can be reduced to $T(R) - T_p \sim (R - R_p)/V_p$ in the limit of strong pinning ($R_p/R_{\rm eq} \ll 1$). This result, averaged over the distribution of pinning radius $P(R)$, is illustrated in Fig. 5

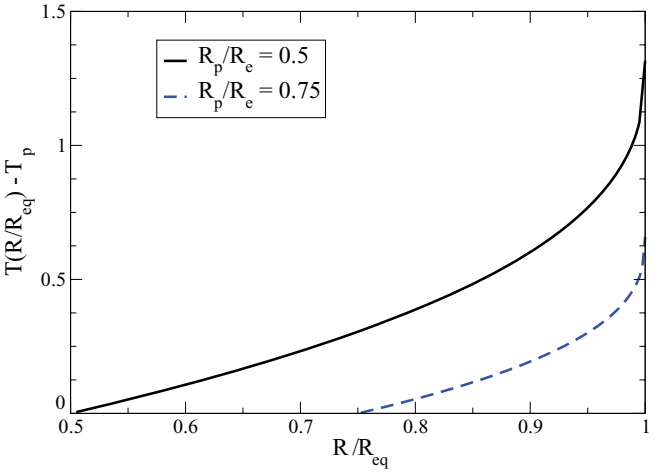

FIG. 5. (Color online) Additional time needed for a spreading droplet to reach the radius $R > R_p$ after reaching R_p [Eq. (26)] for two different values of the ratio $R_p/R_{\rm eq} = 0.5$ and 0.75.

and shows that the time to reach a given $R > R_p$ increases as a function of $R_p/R_{\rm eq}$, particularly for R close to $R_{\rm eq}$.

IV. CONCLUSIONS

To summarize, we have presented a statistical physics theory of droplet asymptotic contact angles on heterogeneous surfaces. This allows us to identify the important quantities, such as the first pinning radius R_p and the ratios to the disorder scale and the equilibrium radius, $R_p/R_{\rm eq}$ and R_p/ξ. The theory presented here applies to droplets with typical lengths above the nanometer scale, such that line tension effects are irrelevant. It is also important that radius variations are smaller than the radius of the droplet, for it to keep a compact circular shape on average. This last requirement implies that the disorder length scale $\xi < R_{\rm eq}$. The contact line dynamics model loses its validity in certain cases—one example is when long-range microscopic forces make it invalid, or when the presence of features such as corrugations make it so that the coarse-grained surface tension indirectly assumed is not present.

Our results predict a dependence of the average contact angle on the volume of the droplet. At constant disorder strength, we expect small droplets to exhibit a markedly larger contact angle at pinning than larger droplets, even more so when the droplet is large with respect to the spatial scale of the disorder. The predictions of the theory can be easily tested through repeated spreading experiments using droplets of different volumes on the same substrate, so that the first pinning radius R_p [cf. Eq. (15)] only depends on the drop volume. It is also possible to test the theory using different liquids on a given surface. Large variations of the apparent contact angle due to the final stage of spreading are expected for small droplets. Many of the consequences of the theory of elastic manifolds are in contrast to static, energy-minimization based results as the Wenzel or Cassie-Baxter laws.

Further theoretical developments include extending the theory presented in this paper to receding radii on hydrophobic surfaces and to develop similar arguments for a structured surface on which gas phase pockets can develop. It is also clear that the theory can be tested through large scale numerical simulations of the relevant hydrodynamics equations. Extending the probabilistic argument to the finite-temperature very-long time creep motion regime, relevant for contact lines as elastic manifolds, is also possible.

ACKNOWLEDGMENTS

We acknowledge the support of the Academy of Finland (via the Center of Excellence program) and TEKES FinNano program via the Silsurf project. M.A. would like to acknowledge the hospitality of Professor E. Frey and the Arnold Sommerfeld Center at the Ludwig-Maximilians-Universität, Munich, Germany.

[1] P. G. de Gennes, Rev. Mod. Phys. **57**, 827 (1985).
[2] J. Eggers, Phys. Rev. E **72**, 061605 (2005).
[3] S. F Kistler, in *Wettability*, edited by J. C. Berg (Dekker, New York, 1993), Chap. 6.
[4] P. G. de Gennes, F. Brochard-Wyart, and D. Quéré, *Capillarity and Wetting Phenomena: Drops, Bubbles, Pearls, Waves* (Springer, New York, 2004).
[5] D. Bonn, J. Eggers, J. Indekeu, J. Meunier, and E. Rolley, Rev. Mod. Phys. **81**, 739 (2009).
[6] D. Quéré, Rep. Prog. Phys. **68**, 2495 (2005).
[7] A. B. D. Cassie and S. Baxter, Trans. Faraday Soc. **40**, 546 (1944).
[8] R. N. Wenzel, Ind. Eng. Chem. **28**, 988 (1936).
[9] T. S. Meiron, A. Marmur, and I. Sam Saguy, J. Colloid Interface Sci. **274**, 637 (2004).
[10] L. Gao and T. J. McCarthy, Langmuir **23**, 3762 (2007).
[11] T. Cubaud and M. Fermigier, J. Colloid Interface Sci. **269**, 171 (2004).
[12] H. Kusumaatmaja and J. M. Yeomans, Langmuir **23**, 956 (2007).
[13] B. M. Mognetti and J. M. Yeomans, Phys. Rev. E **80**, 056309 (2009).
[14] S. Herminghaus, arXiv:1203.5215.
[15] A. Marmur and E. Bittoun, Langmuir **25**, 1277 (2009).
[16] N. Savva, S. Kalliadasis, and G. A. Pavliotis, Phys. Rev. Lett. **104**, 084501 (2010); N. Savva, G. A. Pavliotis, and S. Kalliadasis, J. Fluid Mech. **672**, 358 (2011); **672**, 384 (2011).
[17] J. K. Berg, C. M. Weber, and H. Riegler, Phys. Rev. Lett. **105**, 076103 (2010).
[18] A. Amirfazli and A. W. Neumann, Adv. Colloid Interface Sci. **110**, 121 (2004).
[19] J. F. Joanny and P. G. de Gennes, J. Chem. Phys. **81**, 552 (1984).
[20] M. O. Robbins and J. F. Joanny, Europhys. Lett. **3**, 729 (1987).
[21] F. Brochard-Wyart and P. G. de Gennes, Adv. Colloid Interface Sci. **39**, 1 (1992).
[22] P. Kavehpour, B. Ovrynb, and H. McKinley, Colloids Surf. A **206**, 409 (2002).
[23] C. Yang, U. Tartaglino, and B. N. J. Persson, Eur. Phys. J. B **25**, 139 (2007).
[24] S. Herminghaus, arXiv:1111.4041.
[25] D. Ertas and M. Kardar, Phys. Rev. E **49**, R2532 (1994).
[26] O. Narayan and D. S. Fisher, Phys. Rev. B **48**, 7030 (1993).
[27] R. Golestanian and E. Raphael, Phys. Rev. E **67**, 031603 (2003).
[28] R. David and A. W. Neumann, Langmuir **25**, 13256 (2010).
[29] P. Le Doussal, K. J. Wiese, and P. Chauve, Phys. Rev. B **66**, 174201 (2002).
[30] P. Le Doussal, K. J. Wiese, S. Moulinet, and E. Rolley, Europhys. Lett. **87**, 56001 (2010).
[31] S. Santucci, M. Grob, R. Toussaint, J. Schmittbull, A. Hansen, and K. J. Maloy, Europhys. Lett. **92**, 44001 (2010).
[32] O. Duemmer and W. Krauth, J. Stat. Mech. (2007) P01019.
[33] A. A. Fedorenko, P. Le Doussal, and K. J. Wiese, Phys. Rev. E **74**, 041110 (2006).
[34] Y. Charles, D. Vandembroucq, F. Hild, and S. Roux, J. Mech. Phys. Solids **52**, 1651 (2004).
[35] R. Skoe, D. Vandembroucq, and S. Roux, Int. J. Mod. Phys. C **13**, 751 (2002).